ISSN 1674-1056
http://cpb.iphy.ac.cn
http://iopscience.iop.org/cpb
中国物理 B
Chinese Physics
中国物理 Chinese Physics B

Generalized Drude model and electromagnetic screening in metals and superconductors

Da Wang(王达)
Citation: Chin. Phys. B . 2018, 27(5): 057402. **doi:** 10.1088/1674-1056/27/5/057401

Journal homepage: http://cpb.iphy.ac.cn; http://iopscience.iop.org/cpb

What follows is a list of articles you may be interested in

Two-dimensional electron gas characteristics of InP-based high electron mobility transistor terahertz detector

Jin-Lun Li(李金伦), Shao-Hui Cui(崔少辉), Jian-Xing Xu(徐建星), Xiao-Ran Cui(崔晓然), Chun-Yan Guo(郭春妍), Ben Ma(马奔), Hai-Qiao Ni(倪海桥), Zhi-Chuan Niu(牛智川)

Chin. Phys. B . 2018, 27(4): 047101. **doi:** 10.1088/1674-1056/27/4/047101

Electrical property effect of oxygen vacancies in the heterojunction of $LaGaO_3/SrTiO_3$

Fu-Ning Wang(王芙凝), Ji-Chao Li(李吉超), Xin-Miao Zhang(张鑫淼), Han-Zhang Liu(刘汉璋), Jian Liu(刘剑), Chun-Lei Wang(王春雷), Ming-Lei Zhao(赵明磊), Wen-Bin Su(苏文斌), Liang-Mo Mei(梅良模)
Chin. Phys. B . 2017, 26(3): 037101. **doi:** 10.1088/1674-1056/26/3/037101

Low-resistance Ohmic contact on polarization-dopedAlGaN/GaN heterojunction

Li Shi-Bin, Yu Hong-Ping, Zhang Ting, Chen Zhi, Wu Zhi-Ming
Chin. Phys. B . 2014, 23(10): 107101. **doi:** 10.1088/1674-1056/23/10/107101

Some corrections to the Thomas–Fermi theory

Janusz Chrzanowski
Chin. Phys. B . 2013, 22(8): 087101. **doi:** 10.1088/1674-1056/22/8/087101

Optical spectroscopy studies on $FeTe_{1-x}Se_x$ and $A_xFe_{2-y}Se_2$ (A=K, Rb, Cs)：A brief overview

Yuan Rui-Hua, Wang Nan-Lin
Chin. Phys. B . 2013, 22(8): 087404. **doi:** 10.1088/1674-1056/22/8/087404

Vortex pinning and rectification effect in a nanostructured superconducting film with a square array of antidot triplets*

An He(何安)[1], Cun Xue(薛存)[2,†], and Youhe Zhou(周又和)[3,4]

[1] College of Science, Chang'an University, Xi'an 710064, China
[2] School of Mechanics, Civil Engineering and Architecture, Northwestern Polytechnical University, Xi'an 710072, China
[3] Key Laboratory of Mechanics on Disaster and Environment in Western China attached to the Ministry of Education of China, and Department of Mechanics and Engineering Sciences, Lanzhou University, Lanzhou 730000, China
[4] School of Aeronautics, Northwestern Polytechnical University, Xi'an 710072, China

(Received 5 December 2017; revised manuscript received 5 March 2018; published online 26 April 2018)

We study the stability of vortices pinning and dynamics in a superconducting thin strip containing a square array of antidot triplets by using the nonlinear Ginzburg–Landau (GL) theory. Compared with the regular square array of circular holes, the vortices are no longer pinned inside the circular holes, but instead stabilized at the center of the antidot triplets depending on the geometry parameters. Moreover, the influences of the geometry parameters and the polarity of the applied current on the current–voltage (I–V) characteristics are also studied. The critical current for the sample turning into a normal state becomes smaller when the hole diameter D is smaller and the spacing B between the holes is larger. Due to the asymmetric pinning sites, our numerical simulations demonstrate that the positive and negative rectified voltages appear alternately in the resistive state of the sample under an ac current of square pulses.

Keywords: matching effect, antidot triplets, current–voltage characteristic, critical current

PACS: 74.78.Na, 74.25.Sv, 74.25.Wx, 74.25.N– **DOI:** 10.1088/1674-1056/27/5/057402

1. Introduction

Magnetic flux lines (vortices) in type-II superconductors start to move under an external current, which can result in energy dissipation of the systems and limit the applications of the superconductors. In order to prevent this dissipative motion, it is effective to introduce artificial pinning centers into the superconductors to immobilize the vortices, e.g., chemically grown defects,[1] nanostructured perforations,[2–11] permanent nanomagnets[12–17] or pinning centers produced by irradiation with heavy ions.[18] The superconducting critical parameters can be optimal by tuning the size and magnetization of arrays of magnetic dots.[19,20] It has been found that the critical current of a superconductor can be strongly enhanced at the magnetic field that equals an integer multiple of the number of the periodic pinning sites, i.e., the so-called commensurability effects at the matching fields. Considerable interest has been attracted to enhancing the critical parameters of superconductors with different types of periodic pinning landscapes over the past decades.[2–6,8]

However, it has been recognized that the enhancement of the critical current by uniform pinning arrays becomes less effective at magnetic fields unequal to the matching fields. Many efforts have been made to overcome this shortcoming at incommensurate fields. More complicated pinning landscapes such as Penrose lattice arrays,[21–24] honeycomb arrays,[25,26] or graded pinning landscapes[27–29] were proposed to enhance the critical current of the samples. Latimer *et al.*[26] reported that the commensurability effect for the superconducting film with a honeycomb array of holes occurs at magnetic fields $H/H_1 = n + 1/2$ (n is an integer and H_1 is the first matching field where the number of vortices equals to the number of pins), which is distinguished from the pinning phenomena of the regular square array of holes. In Ref. [30], the anomalous matching effect in a square ice arrangement was studied and the critical current at the half matching field was even higher than that at zero field. For a similar geometry, the field-matching effects could be switched on or off by the temperature.[31] This provides a handle to controllably introduce defects via temperature variations. In addition, both theoretical and experimental results demonstrated that conformal crystal arrays can enhance the pinning of vortices.[32–34] Recently, Wang *et al.*[35] demonstrated that the pinning effects of randomly distributed nanoscale holes patterned into superconducting films can enhance the superconducting critical currents over a wider magnetic field range than the periodic pinning holes. Berdiyorov *et al.*[36] studied the effect of ordered and random pinnings on the time response of superconducting strips to an external current. Weak pinning centers were studied and a variety of vortex states could be stabilized by decreasing the pinning strength of the antidots.[37] In addition to

*Project supported by the National Natural Science Foundation of China (Grant Nos. 11702034, 11702218, and 11421062), Fundamental Research Funds for the Central Universities, China (Grant Nos. 310812171011 and G2016KY0305), and the National Key Project of Magneto-Constrained Fusion Energy Development Program, China (Grant No. 2013GB110002).

†Corresponding author. E-mail: xuecun@nwpu.edu.cn

© 2018 Chinese Physical Society and IOP Publishing Ltd

the permanent pinning landscapes, a dynamical pinning landscape was proposed and triggered new phenomena.[38,39]

Substantial works have been devoted to studying the commensurability effects in the systems with various types of perforated antidots. Moreover, the vortex-rectification effects in superconducting films with asymmetric pinning have been reported.[40–43] Rectification by an imprinted phase in a Josephson junction was proposed.[44] Motivated by these studies, we aimed to investigate the properties of samples with a square array of antidot triplets. The antidot triplets act as one pinning site to stabilize the vortices. The influence of the size and spacing of the circular antidots on the critical currents is presented. It is found that the critical parameters and transport properties of such a sample can be strongly dependent on the geometry parameters. As the pinning sites considered in this paper are asymmetric, the polarity of the applied current can have a great impact on the *I*–*V* characteristics of the sample. The vortex rectification effect can be observed when the sample is subjected to an ac current.

The paper is organized as follows. In Section 2, we present the details of our numerical formalism. Section 3 deals with the vortex lattices in the perforated films in a homogeneous magnetic field, and the numbers of pinned and interstitial vortices with different antidot sizes and different interhole distances are shown. Moreover, the electric properties of the sample by changing the geometry parameters are discussed. And the vortex rectification effect by considering an ac current made of square pulses is presented. In Section 4, all presented findings are summarized.

2. Theoretical approach

We consider a thin (thickness $d \ll \xi$, λ) superconducting strip with an array geometry of circular holes (diameter D) under the applied magnetic field $H = H_a/H_{c2}$ (shown in Fig. 1(a)). The array geometry is characterized by three parameters A, B, and D (denoted by A–B–D), which can be considered as a square array of antidot triplets. To compare the array geometry, we also conduct simulations with a regular square array of holes A–D (period A and diameter D) shown in Fig. 1(b). In order to investigate the vortex arrangement at various magnetic fields, we perform our simulations for the ground-state vortex configurations within the Ginzburg–Landau (GL) theory by solving the time-dependent GL (TDGL) equations in the zero electrostatic potential gauge. To explore the dynamic properties in superconducting film, an external current I is applied along the x direction after the ground state. Then the vortex lattice becomes rearranged by the external current. In order to model both dynamic and static superconducting properties, the normalized TDGL equations can be written as[45–47]

$$\frac{\partial \psi}{\partial t} = (\nabla - \mathrm{i}\boldsymbol{A})^2\psi + \psi - |\psi|^2\psi, \tag{1}$$

$$\sigma\frac{\partial \boldsymbol{A}}{\partial t} = \boldsymbol{J}_s - \kappa^2\nabla\times\nabla\times\boldsymbol{A}, \tag{2}$$

$$\boldsymbol{J}_s = \mathrm{Im}(\psi^*\nabla\psi) - \boldsymbol{A}|\psi|^2, \tag{3}$$

where ψ, $\boldsymbol{A}$, and $\boldsymbol{J}_s$ are the order parameter, the vector potential, and the supercurrent density, respectively. In these equations, the length is made dimensionless in units of coherence length $\xi(t)$, time in $t_0 = \pi\hbar/8k_B(T_c - T)$, vector potential $\boldsymbol{A}$ in $H_{c2}\xi$, and the magnetic field is scaled by $H_{c2} = \Phi_0/2\pi\xi^2$ (where Φ_0 is the magnetic flux quantum). The magnitude of the applied magnetic field $H_n = n\Phi_0/S$ is determined by the number n of flux quanta piercing through the rectangular simulation area $S = L \times L$. The voltage is in units of $V_0 = c\Phi_0\rho_n/8\pi^2\lambda\xi$, where ρ_n is the normal-state resistivity and the current density is scaled by $j_0 = c\Phi_0/8\pi^2\lambda^2\xi$.

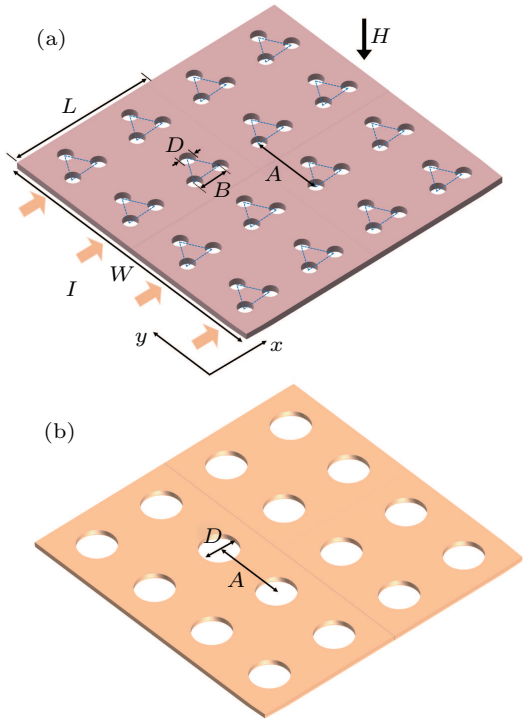


Fig. 1. (color online) Schematic view of thin superconducting strip with array of holes. (a) One array geometry is characterized by two distances A (the period of the antidot triplets), B (the spacing among the antidot triplets), and the hole diameter D (denoted by A–B–D). (b) Another array geometry is characterized by the square period A and the hole diameter D (denoted by A–D).

The Gibbs free energy of the superconducting system can be written as

$$G_t = V^{-1}\int_V [2(\boldsymbol{A} - \boldsymbol{A}_0)\boldsymbol{J}_s - |\psi|^4]\,\mathrm{d}\boldsymbol{r}, \tag{4}$$

where integration is performed over the sample volume V, and $\boldsymbol{A}_0$ is the vector potential of the uniform magnetic field. Because the thickness of the sample is sufficiently thin, the variations of the order parameter and currents along the thickness are neglected in the simulations.

For the quasi-static vortex simulations, our simulation region is a $2L \times 2L$ square with 4×4 unit cells. The periodicity of the sample is included through the boundary conditions for $\boldsymbol{A}$ and ψ in the form $\boldsymbol{A}(\boldsymbol{r}+\ell_i) = \boldsymbol{A}(\boldsymbol{r}) + \nabla\zeta_i(\boldsymbol{r})$ and $\psi(\boldsymbol{r}+\ell_i) = \psi\exp(2\pi \mathrm{i}\,\zeta_i(\boldsymbol{r})/\Phi_0)$, where $\ell_{i=x,y}$ are the lattice vectors, and ζ_i is the gauge potential. We use the Landau gauge $\boldsymbol{A}_\mathrm{a} = Hx\boldsymbol{e}_y$ for the vector potential. We discrete the equations applying the finite-difference method on a uniform 2D Cartesian space grid and use the Euler iterative methods to solve the TDGL equation (1), and the vector potential is obtained with the fast Fourier transform technique.

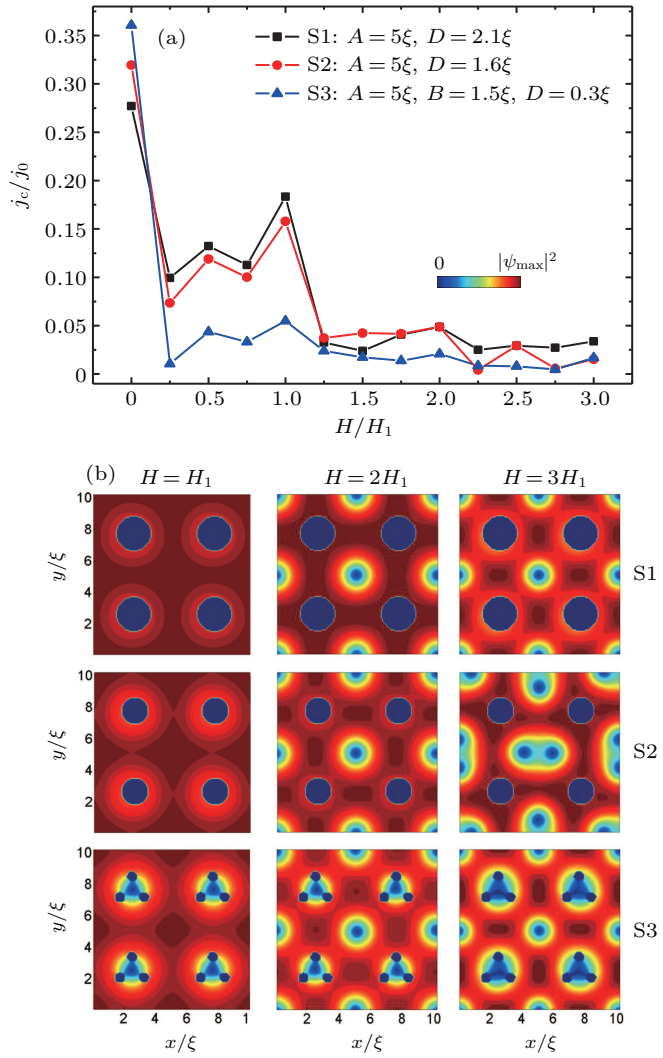


Fig. 2. (color online) (a) Normalized critical current density as a function of applied magnetic field (in units of the first matching field H_1 in the *A*–*D* array) for the two array geometries of holes. (b) The contour plots of the simulated ground state vortex configurations at the first, second, and third matching fields for different arrays of *A*–*D* (S1, S2)) and the array *A*–*B*–*D* (S3).

For the dynamic properties of the superconducting strip, our simulation region is an $L \times W$ rectangular with 2×4 unit cells. The infinite sample is implemented through periodic boundary condition $\psi(x,y) = \psi(x+L,y)$ and $\boldsymbol{A}(x,y) = \boldsymbol{A}(x+L,y)$ in the x direction. The superconducting–vacuum boundary condition $(\nabla - \mathrm{i}\boldsymbol{A})\psi|_{x=0,W} = 0$ is used in the x direction. The current is applied via the boundary conditions $\mathrm{rot}\ \boldsymbol{A}|_z(x=0,W) = H \pm H_I$ for the vector potential, where $H_I = 2\pi I/c$ is the magnetic field induced by the current I. In the present simulations, we take $\xi = 22$ nm and $\lambda = 44$ nm at zero temperature and all our simulations are implemented at the working temperature $0.95T_\mathrm{c}$.

3. Numerical results

We investigate the above arrays by calculating the critical current versus magnetic field. It is known that the vortices form highly ordered configurations in samples with periodic pinning centers at the integer field. Firstly, we consider the case of sample *A*–*D* with $D = 2.1\xi$ (S1) and $D = 1.6\xi$ (S2) with the same array period A. It can be seen from Fig. 2 that the vortex configurations of S1 and S2 exhibit well-defined matching phenomena, which result in the pronounced critical current. Due to the larger holes in S1, two vortices can be pinned by the holes, i.e., the hole occupation number $n_0 = 2$ at the third matching field, while for S2 with small hole radius, the hole occupation number is $n_0 = 1$. Thus, there are more additional vortices located in the interstitial site at the same magnetic field, which can reduce the critical current. In contrast, the holes in sample *A*–*D* are much larger than those in sample *A*–*B*–*D*, i.e., the diameter D in sample *A*–*D* can be analogous to the sum of the parameters B and D in sample *A*–*B*–*D*. This can be used to analyze the vortex configuration and critical current at the same field between the two types of samples. For the case of sample *A*–*B*–*D*, the matching effect is not obvious compared with the case of sample *A*–*D*. This is due to that the unit cell comprised of the three small holes stabilizes the vortices in the center of the triangular. This feature is similar to the principle in Ref. [31], where Trastoy *et al.* reported that the vortices are located in the middle of the pairwise holes and it seems that the vortices are located in the oval pinning sites. Thus the vortices cannot be pinned inside the holes. This implies that the three holes close to each other act as one pinning site, and the energy of the system is minimal when the vortices are located at the center. Whether the vortices are pinned in holes or located at the center of the antidot triplets mainly depends on the competition between the pinning force by one hole and the attractive forces by two nearest-neighboring holes by supposing a vortex pinned in the hole. Therefore, the vortex states at H_1 are mainly determined by the spacing between holes since the parameter B can change the attractive force but it has no impact on the pinning force. Comparing sample *A*–*D* with sample *A*–*B*–*D*, one can see that the vortex configuration in S3 is similar with that in S1. However, the critical currents $j_\mathrm{c}(H_i)$ $(i = 1,2,3)$ of sample S1 at the matching field are much larger than those of sample S3. This can be attributed to that the pinning strength of vortices are largely weakened in S3.

Therefore, the critical current cannot be enhanced by increasing the density of the pinning sites.

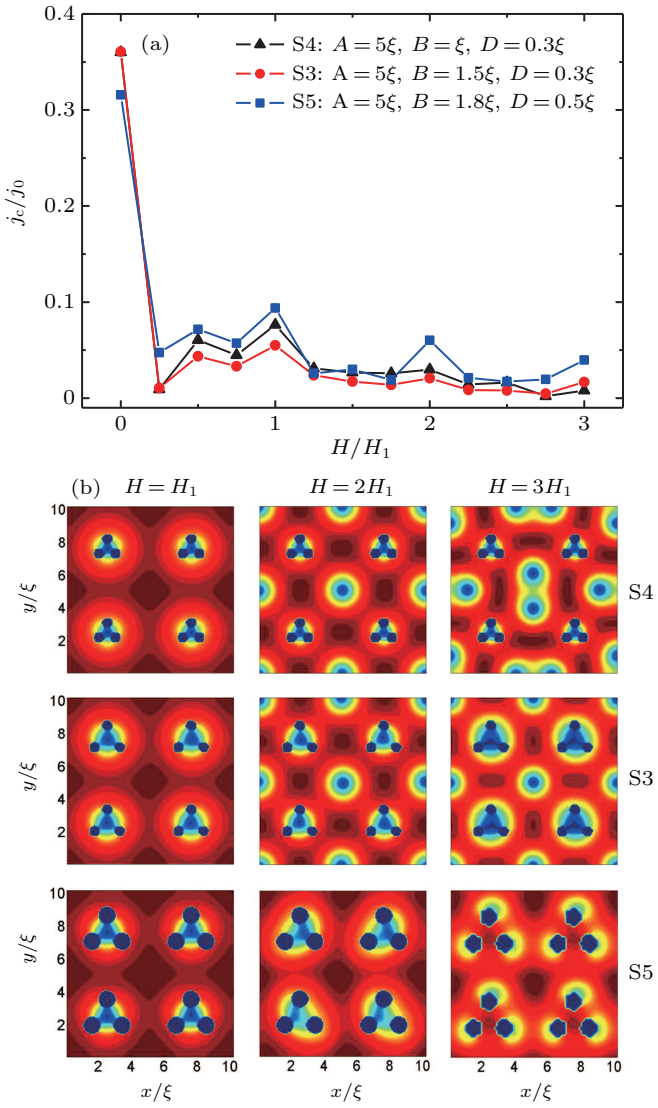


Fig. 3. (color online) (a) Normalized critical current density as a function of applied magnetic field (in units of H_1 in the *A*–*D* array) for three samples with different arrays of *A*–*B*–*D*. The film thickness is $d=0.25\xi$. (b) The ground-state vortex configurations at the first, second, and third matching fields.

We now focus on the critical parameters of the sample *A*–*B*–*D* at different magnetic fields shown in Fig. 3. For the same parameters *A* and *D* in S3 and S4, as the length of the triangle *B* becomes larger, the pinning strength is much weaker, which leads to a smaller critical current at $H \leq H_2$. While at $H = H_3$ there are more vortices stabilized by the antidot triplets in S3 than that in S4, which results in a little larger critical current. When the hole diameter also becomes larger, sample S5 can not only stabilize the vortices in the center of the antidot triplets but also pin three vortices in each hole at $H = H_3$. Thus the critical current of S5 is the largest among the three samples. Such vortex state is due to the competition between the vortex–vortex interaction and the vortex–hole interaction. On the other hand, if the magnetic field is scaled by the first matching field H_1 in the *A*–*B*–*D* array, the critical current at the integer matching field is much smaller than that at the fractional matching field.

To demonstrate the influence of hole diameter *D* and array period *B* on the vortex motion, in what follows, we investigate the response of such system to an external current and perpendicular magnetic field. Figure 4(a) shows the *I*–*V* characteristics of the three samples *A*–*B*–*D* with different parameters at $H = 0.6$. The sample keeps the superconducting state before the external current reaches the first critical current $I_{c1} = 0.0155$ for the sample 2.5ξ–1.5ξ–0.2ξ, at which two vortices enter the sample one by one from the top edge (Fig. 4(b)). As the applied current exceeds I_{c1}, the sample turns into the resistive state where two vortices penetrate the sample and move synchronously (Fig. 4(c)). For the sample with smaller *D* and larger *B*, it is more favorable to induce moving vortices, which leads to a smaller critical current. As the applied current reaches the second critical current $I_{c2} = 0.1293$ for the sample 2.5ξ–1.5ξ–0.2ξ, the sample transits into a higher resistivity which becomes a normal state (Fig. 4(d)). For another sample 2.5ξ–1.5ξ–0.3ξ with larger diameter, the resistive state of the sample is put off (Fig. 4(e)) and the critical current of the sample into a normal state is larger (Fig. 4(f)). To conclude, we demonstrate that when the sample has larger *D* and smaller *B*, the critical current for the transition of the sample into normal state is much larger.

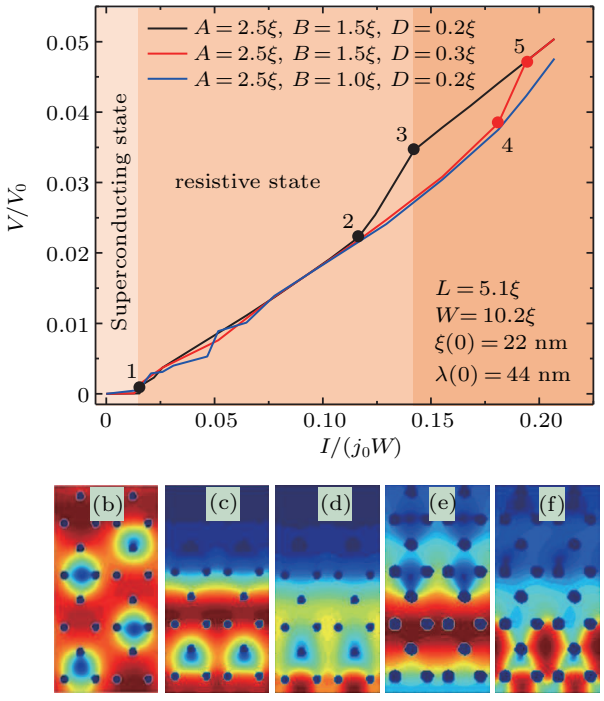


Fig. 4. (color online) Current–voltage characteristics of three samples with different arrays *A*–*B*–*D* under the applied field $H = 0.6$. Panels (b)–(f) show snapshots of Cooper-pair density for currents 1–5 indicated on the *I*–*V* curves.

As the geometry of the pinning sites considered in this paper with respect to the *x* direction is asymmetric, we demon-

strate the impact of the polarity of the external current on the I–V characteristics. Figure 5(a) shows the time evolution of the voltage under an ac current made of square pulses with amplitude $I_{ac}/(j_0W) = 0.1423$. It can be seen that the output voltage in the first half-period with I_{ac} is different from that in the second half-period with $-I_{ac}$ during each full cycle. The sample turns into the normal state for a positive x direction current. However, it keeps the resistive state at the negative x direction current and the inset shows the enlargement of voltage oscillation with time. Thus, the critical current for the sample turning into normal state is larger for the sample under $-I_{ac}$. The nonzero average voltage during one period in the $V(t)$ curve exhibits an important feature of the sample, i.e., the vortex rectification can be observed when the sample is subjected to an ac current. Figure 5(b) shows the rectification effect for the sample 2.5ξ–1.5ξ–0.2ξ at field $H = 0.6$. One can see that the positive and negative rectified voltages appear, and the maximum rectification effects correspond to the three peaks of the V_{dc}–I_{ac} curves. In the rectification window, the dc voltage of the asymmetric samples reaches zero at low and high ac drives. This indicates that there is no vortex ratchet effect when the sample keeps the superconducting state and normal state. Consequently, the rectified voltage can be tuned by the amplitude of the ac current, which is reminiscent to the controlled multiple reversals of a ratchet effect observed in superconductors with asymmetric double-well potentials.[42]

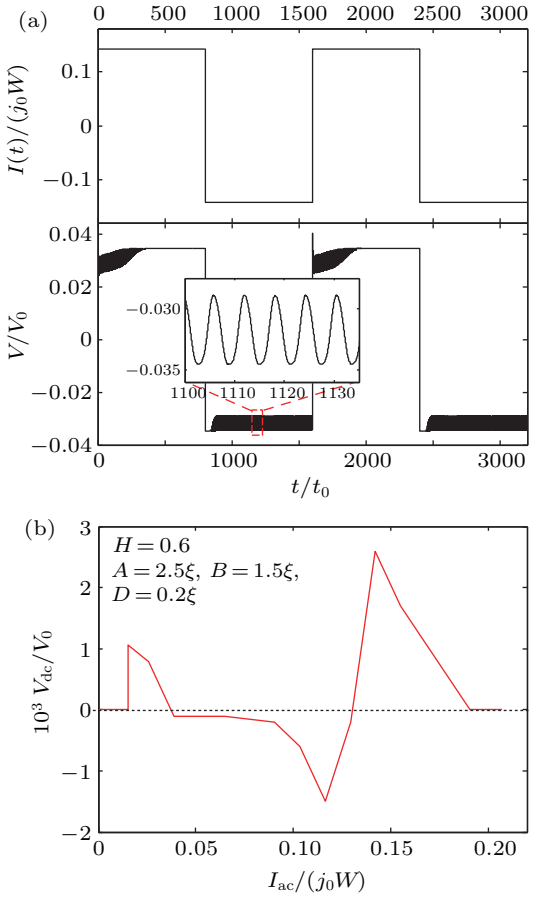


Fig. 5. (color online) (a) The voltage versus time response (bottom) under an ac current made of square pulses with amplitude $I_{ac}/(j_0W) = 0.1423$ (top). The inset shows the enlargement of voltage oscillation vs. time. (b) Normalized dc voltage of the sample versus current amplitude at $H = 0.6$.

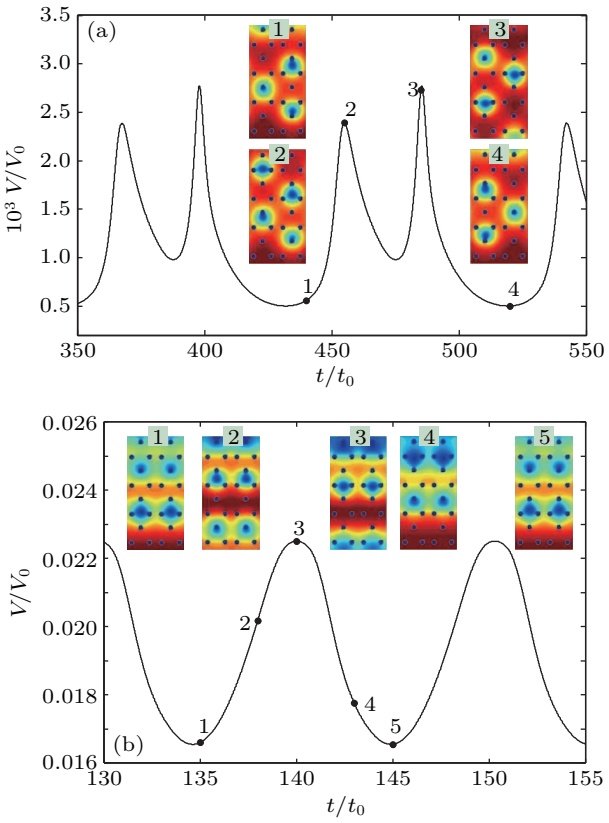


Fig. 6. (color online) Equilibrated voltage versus time response of the sample with the array geometry $A = 2.5\xi$, $B = 1.5\xi$, $D = 0.2\xi$ at $I/(j_0W) = 0.0155$ (a) and 0.1 (b) under the applied field $H = 0.6$. The insets show snapshots of Cooper-pair density at time indicated in the $V(t)$ curve.

Lastly, we would like to discuss the $V(t)$ curves of sample 2.5ξ–1.5ξ–0.2ξ for $I/(j_0W) = 0.0155$ and 0.1 at $H = 0.6$. The snapshots of the Cooper-pair density are also presented to show the time evolution of the superconducting condensate. At small current shown in Fig. 6(a), the output voltage oscillates with time, and two local extremes are observed at each period. One vortex penetrates into the sample from the top left corner at the global minimal voltage (inset 1). Then the vortices move along the two vertical columns (inset 2) in the form of a triangular lattice until the disappearance of the vortex at the maximum of voltage oscillation (inset 3). Another vortex enters the sample from the top right corner (inset 4) and the system continues the similar dynamical process. It can be observed that vortices penetrate into the sample one by one and move along each vertical column, which leads to the larger time period of the vortices motion. The applied current is so large that two vortices can penetrate the sample simultaneously shown in Fig. 6(b). This leads to the minimal measured voltage (inset 1). Then the vortices move downward

(inset 2) until they exit the sample synchronously (inset 3) at the maximum value. The remaining vortices continue moving in the sample (inset 4). As time goes on, new vortices enter the sample (inset 5), beyond which the superconducting condensate relaxes toward next dynamical process. It should be mentioned that the average vortex velocity (sample width divided by time between vortex entry and exit) $v \approx 8.7$ km/s at $I/(j_0 W) = 0.1$. Experiments on Pb samples showed the extreme values of vortex velocities of 10–20 km/s.[48] This implies that the vortex motion is slowed down by the pinning sites by referring to the measured vortex velocities.

4. Conclusions

In summary, we study the magnetic field dependence of the critical current and transport properties of a superconducting strip containing a square array of antidot triplets within the GL theory. Different from the vortices pinned by the holes in a regular square lattice, our results show that the vortices can no longer be trapped inside the circular holes, but are stabilized at the center of the antidot triplets, which depends on the geometry parameters. Whether vortices are pinned in holes or located at the center of the antidot triplets mainly depends on the spacing between holes B. The impacts of the geometry parameters and the polarity of the applied current on the I–V characteristics are also studied. It is found that the critical current I_{c2} for the sample turning into normal state becomes smaller when the hole diameter D is smaller and B is larger. Furthermore, the sample can exhibit the feature of vortex rectification when it is subjected to an ac current. The positive and negative rectified voltages can be observed alternately with the increasing amplitude of the ac current. The rectification effect appears in the resistive state of the sample and the current amplitude is restricted in the range between the first critical current I_{c1} for the sample turning into resistive state and the second critical current I_{c2}.

References

[1] Macmanus-Driscoll J L 2004 *Nat. Mater.* **3** 439
[2] Welp U, Xiao Z L, Jiang J S, Vlasko-Vlasov V K, Bader S D, Crabtree G W, Liang J, Chik H and Xu J M 2002 *Phys. Rev. B* **66** 212507
[3] Berdiyorov G R, Milošević M V and Peeters F M 2006 *Phys. Rev. Lett.* **96** 207001
[4] Berdiyorov G R, Milošević M V and Peeters F M 2006 *Europhys. Lett.* **74** 493
[5] Berdiyorov G R, Milošević M V and Peeters F M 2006 *Phys. Rev. B* **74** 174512
[6] Silhanek A V, Van Look L, Jonckheere R, Zhu B Y, Raedts S and Moshchalkov V V 2005 *Phys. Rev. B* **72** 014507
[7] Kemmler M, Bothner D, Ilin K, Siegel M, Kleiner R and Koelle D 2009 *Phys. Rev. B* **79** 184509
[8] Rablen S, Kemmler M, Quaglio T, Kleiner R, Koelle D and Grigorieva I V 2011 *Phys. Rev. B* **84** 184520
[9] Swiecicki I, Ulysse C, Wolf T, Bernard R, Bergeal N, Briatico J, Faini G, Lesueur J and Villegas J E 2012 *Phys. Rev. B* **85** 224502
[10] Reichhardt C, Zimanyi G T, Scalettar R T, Hoffmann A and Schuller I K 2001 *Phys. Rev. B* **64** 052503
[11] Adami O A, Jelic Z L, Xue C, Abdel-Hafiez M, Hackens B, Moshchalkov V V, MiloševićMV, Van de V J and Silhanek A V 2015 *Phys. Rev. B* **92** 134506
[12] Milošević M V and Peeters F M 2004 *Phys. Rev. B* **69** 104522
[13] Milošević M V and Peeters F M 2003 *Phys. Rev. B* **68** 094510
[14] Kramer R B G, Silhanek A V, Gillijns W and Moshchalkov V V 2011 *Phys. Rev. X* **1** 021004
[15] Milošević M V, Gillijns W, Silhanek A V, Libál A, Peeters F M and Moshchalkov V V 2010 *Appl. Phys. Lett.* **96** 032503
[16] Silhanek A V, Gillijns W, Moshchalkov V V, Metlushko V and Ilic B 2006 *Appl. Phys. Lett.* **89** 182505
[17] Van Bael M J, Lange M, Raedts S, Moshchalkov V V, Grigorenko A N and Bending S J 2003 *Phys. Rev. B* **68** 014509
[18] Maiorov B 2009 *Nat. Mater.* **8** 398
[19] Silhanek A V, Gillijns W, Milošević M V, Volodin A, Moshchalkov V V and Peeters F M 2007 *Phys. Rev. B* **76** 100502
[20] Gillijns W, Milošević M V, Silhanek A V, Moshchalkov V V and Peeters F M 2007 *Phys. Rev. B* **76** 184516
[21] Misko V R, Bothner D, Kemmler M, Kleiner R, Koelle D, Peeters F M and Nori F 2010 *Phys. Rev. B* **82** 184512
[22] Kramer R B G, Silhanek A V, Van de Vondel J, Raes B and Moshchalkov V V 2009 *Phys. Rev. Lett.* **103** 067007
[23] Silhanek A V, Gillijns W, Moshchalkov V V, Zhu B Y, Moonens J and Leunissen L H A 2006 *Appl. Phys. Lett.* **89** 152507
[24] Silhanek A V, Gillijns W, Moshchalkov V V, Zhu B Y, Moonens J and Leunissen L H A 2006 *Appl. Phys. Lett.* **89** 152507)
[25] Reichhardt C and Olson Reichhardt C J 2008 *Phys. Rev. Lett.* **100** 167002
[26] Latimer M L, Berdiyorov G R, Xiao Z L, Kwok W K and Peeters F M 2012 *Phys. Rev. B* **85** 012505
[27] Gillijns W, Silhanek A V, Moshchalkov V V, Olson Reichhardt C J and Reichhardt C 2007 *Phys. Rev. Lett.* **99** 247002
[28] Misko V R and Nori F 2012 *Phys. Rev. B* **85** 184506
[29] Motta M, Colauto F, OrtizWA, Fritzsche J, Cuppens J, GillijnsW, Moshchalkov V V, Johansen T H, Sanchez A and Silhanek A V 2013 *Appl. Phys. Lett.* **102** 212601
[30] Latimer M L, Berdiyorov G R, Xiao Z L, Peeters F M and Kwok W K 2013 *Phys. Rev. Lett.* **111** 067001
[31] Trastoy J, Malnou M, Ulysse C, Bernard R, Bergeal N, Faini G, Lesueur J, Briatico J and Villegas J E 2014 *Nat. Nanotech.* **9** 710
[32] Ray D, Olson Reichhardt C J, Janko B and Reichhardt C 2013 *Phys. Rev. Lett.* **110** 267001
[33] Wang Y L, Latimer M L, Xiao Z L, Divan R, Ocola L E, Crabtree G W and Kwok W K 2013 *Phys. Rev. B* **87** 220501
[34] Guénon S, Rosen Y J, Basaran Ali C and Schuller Ivan K 2013 *Appl. Phys. Lett.* **102** 252602
[35] Wang Y L, Thoutam L R, Xiao Z L, Shen B, Pearson J E, Divan R, Ocola L E, Crabtree G W and Kwok W K 2016 *Phys. Rev. B* **93** 045111
[36] Berdiyorov G R, Harrabi K, Maneval J P and Peeters F M 2015 *Supercond. Sci. Technol.* **28** 025004
[37] Berdiyorov G R, Milošević M V and Peeters F M 2007 *Phys. Rev. B* **76** 134508
[38] Jelic Z L, Milošević M V, Van de Vondel J and Silhanek A V 2015 *Sci. Rep.* **5** 14604
[39] Jelic Z L, Milošević M V and Silhanek A V 2016 *Sci. Rep.* **6** 35687
[40] Villegas J E, Savelev S, Nori F, Gonzalez E M, Anguita J V, Garcia R and Vicent J L 2003 *Science* **302** 1188
[41] Van de Vondel J, de Souza Silva C C, Zhu B Y, Morelle M and Moshchalkov V V 2005 *Phys. Rev. Lett.* **94** 057003
[42] de Souza Silva C C, Van de Vondel J, Morelle M and Moshchalkov V V 2006 *Nature* **440** 651
[43] Van de Vondel J, Gladilin V N, Silhanek A V, Gillijns W, Tempere J, Devreese J T and Moshchalkov V V 2011 *Phys. Rev. Lett.* **106** 137003
[44] Berdiyorov G R, Milošević M V, Covaci L and Peeters F M 2011 *Phys. Rev. Lett.* **107** 177008
[45] Gropp W D 1996 *J. Comput. Phys.* **123** 254
[46] Schweigert V A and Peeters F M 1998 *Phys. Rev. B* **57** 13817
[47] Winiecki T and Adams C S 2002 *J. Comput. Phys.* **179** 127
[48] Embon L, Anahory Y, Jelic Z L, Lachman E O, Myasoedov Y, Huber M E, Mikitik G P, Silhanek A V, Milošević M V, Gurevich A and Zeldov E 2017 *Nat. Commun.* **8** 85